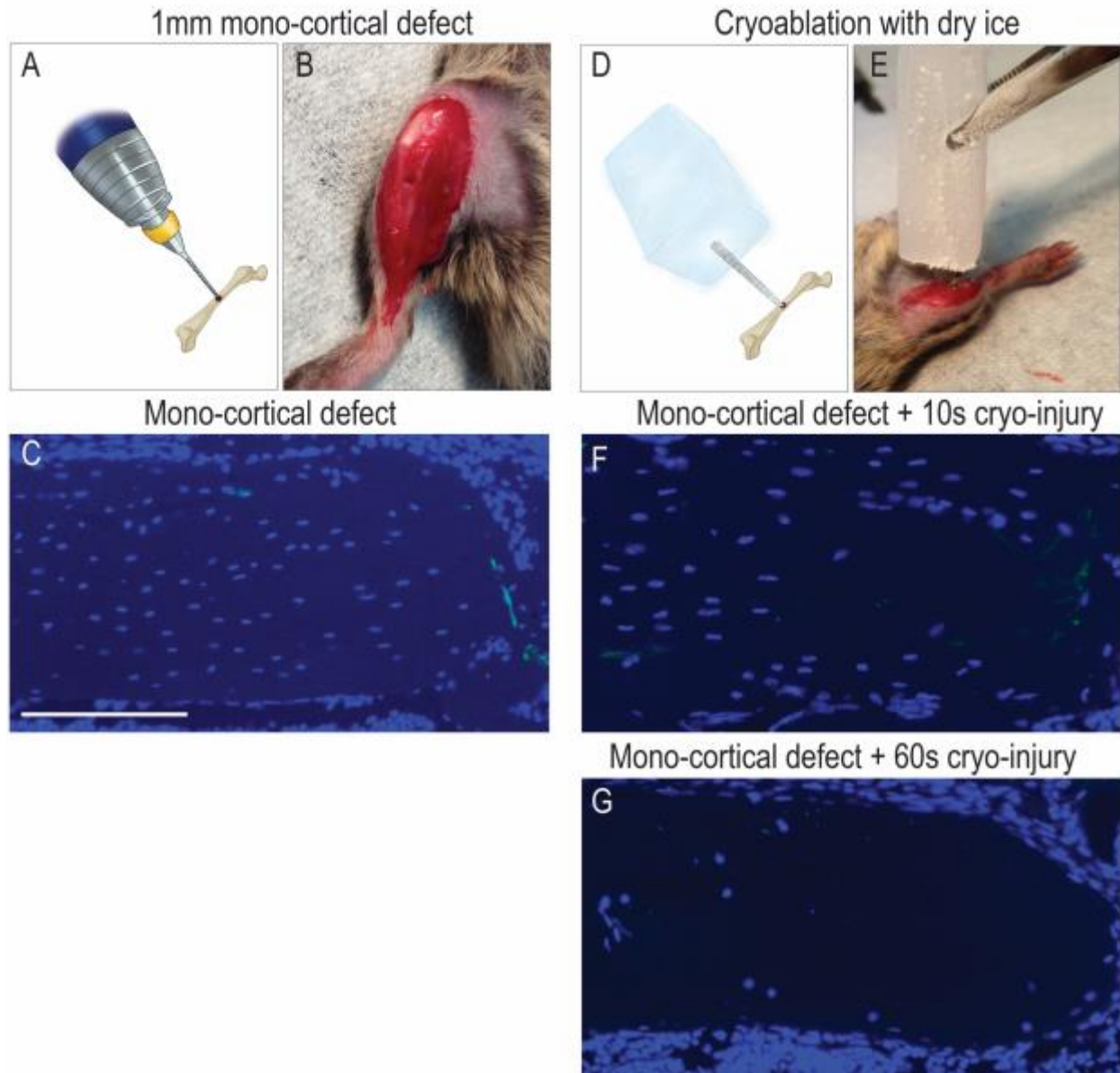


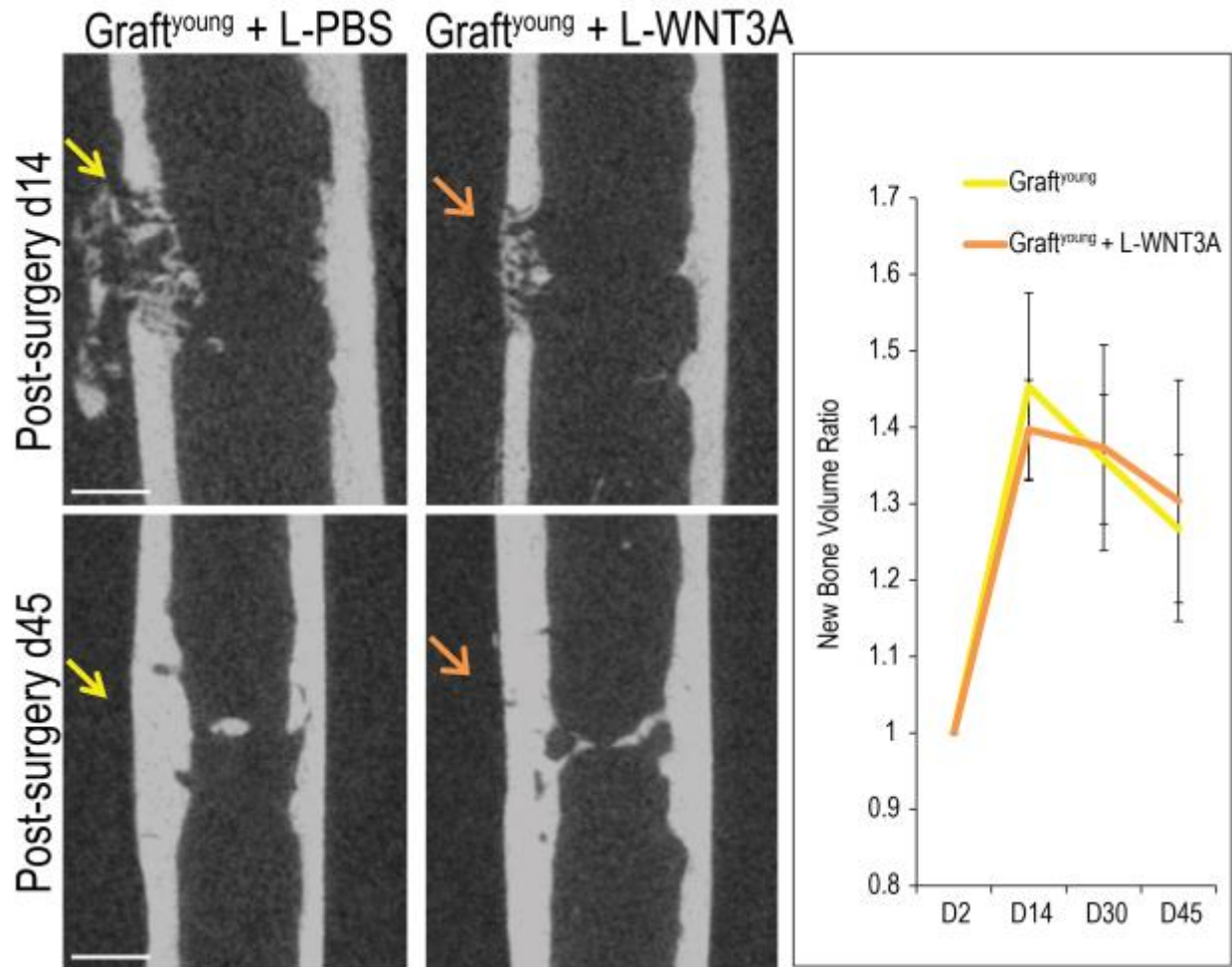
WNT-activated bone grafts repair osteonecrotic lesions in aged animals

Salmon B^{1,2}, Liu B¹, Shen E¹, Chen T^{1,3}, Li J^{1,3}, Gillette M¹, Ransom RC¹, Ezran M¹, Johnson CA^{1,4}, Castillo AB⁵,
Shen WJ⁶, Kraemer FB⁶, Smith AA¹, Helms JA*¹



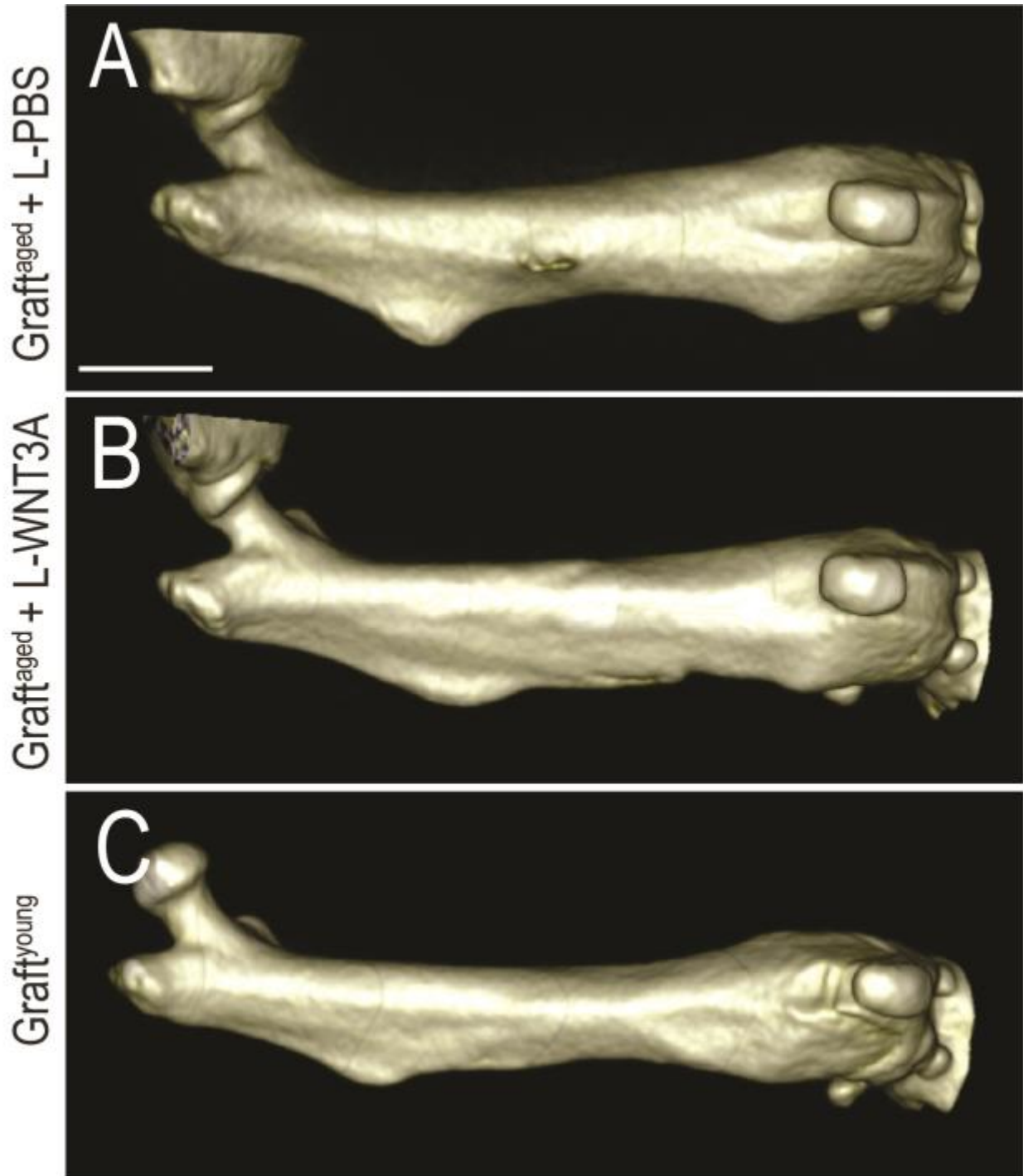
Supplemental Figure 1. Schematic of the osteonecrotic mouse model and confirmation of cell death by cryoablation.

(A,B) To expose the bone marrow space, a mono-cortical defect is performed in either the femur or tibia using a calibrated 1.0mm diameter drill. (C) DAPI staining focusing on the cortical edge of the defects, reveals the distribution of viable osteocytes. (D,E) To create necrosis of the bone a 1.0mm diameter drill is used as a cryo-probe to conduct the low-temperature from the dry ice to the defect. DAPI staining shows remaining viable osteocyte nuclei inside the cortical edge after (F) 10sec and (G) 60sec of cryoablation. Scale bars, 100 μ m; same magnification was applied in panels C,F,G.



Supplemental Figure 2. Graft^{young} and graft^{young} + L-WNT3A perform equivalently in healing osteonecrotic defects.

Micro-CT image quantification from post surgery days 14 and 45 show similar extents of healing between those animals receiving graft^{young} + L-PBS and those treated with graft^{young} + L-WNT3A. Scale bars, 0.5mm; same magnification was applied in all panels.



Supplemental Figure 3. Bone grafting results in healing of osteonecrotic defects.

On post-surgery day 30 surface rendering showed nearly detectable concavities associated with the osteonecrotic defects, although slight surface irregularities were detected in animals treated with

graft^{aged}. No ectopic bone was detected in any treatment group ($N \geq 4$ for each condition). (A) graft^{aged} + L-PBS, (B) graft^{aged} + L-WNT3A and (C) graft^{young}. Scale bars, 2mm; same magnification was applied in panels A-C.